Report

Current Biology

Role of Corticotropin-Releasing Factor in Cerebellar Motor Control and Ataxia

Highlights

- Deficiency of CRF in the inferior olive induces ataxia-like motor abnormalities
- CRFergic neurons in the inferior olive project directly to the cerebellar nuclei
- CRF selectively excites the cerebellar nuclear glutamatergic projection neurons
- CRF promotes cerebellar motor coordination and rescues ataxic motor deficits

Authors

Yi Wang, Zhang-Peng Chen, Qian-Xing Zhuang, Xiao-Yang Zhang, Hong-Zhao Li, Jian-Jun Wang, Jing-Ning Zhu

Correspondence

jjwang@nju.edu.cn (J.-J.W.), jnzhu@nju.edu.cn (J.-N.Z.)

In Brief

CRF is a critical neurotransmitter implicated in stress and anxiety. Wang et al. define a direct functional role for CRF in the olivo-cerebellar system in motor coordination via selective modulation on cerebellar nuclear glutamatergic projection neurons, and provide new insight into the etiology and treatment strategy of cerebellar ataxia.

Wang et al., 2017, Current Biology *27*, 1–9
September 11, 2017
http://dx.doi.org/10.1016/j.cub.2017.07.035

CellPress

Please cite this article in press as: Wang et al., Role of Corticotropin-Releasing Factor in Cerebellar Motor Control and Ataxia, Current Biology (2017), http://dx.doi.org/10.1016/j.cub.2017.07.035

Current Biology
Report

Role of Corticotropin-Releasing Factor in Cerebellar Motor Control and Ataxia

Yi Wang,[1,2] Zhang-Peng Chen,[1,2] Qian-Xing Zhuang,[1,2] Xiao-Yang Zhang,[1] Hong-Zhao Li,[1] Jian-Jun Wang,[1,*] and Jing-Ning Zhu[1,3,*]
[1]State Key Laboratory of Pharmaceutical Biotechnology and Department of Biological Science and Technology, School of Life Sciences, Nanjing University, 163 Xianlin Avenue, Nanjing 210023, China
[2]These authors contributed equally
[3]Lead Contact
*Correspondence: jjwang@nju.edu.cn (J.-J.W.), jnzhu@nju.edu.cn (J.-N.Z.)
http://dx.doi.org/10.1016/j.cub.2017.07.035

SUMMARY

Cerebellar ataxia, characterized by motor incoordination, postural instability, and gait abnormality [1–3], greatly affects daily activities and quality of life. Although accumulating genetic and non-genetic etiological factors have been revealed [4–7], effective therapies for cerebellar ataxia are still lacking. Intriguingly, corticotropin-releasing factor (CRF), a peptide hormone and neurotransmitter [8, 9], is considered a putative neurotransmitter in the olivo-cerebellar system [10–14]. Notably, decreased levels of CRF in the inferior olive (IO), the sole origin of cerebellar climbing fibers, have been reported in patients with spinocerebellar degeneration or olivopontocerebellar atrophy [15, 16], yet little is known about the exact role of CRF in cerebellar motor coordination and ataxia. Here we report that deficiency of CRF in the olivo-cerebellar system induces ataxia-like motor abnormalities. CRFergic neurons in the IO project directly to the cerebellar nuclei, the ultimate integration and output node of the cerebellum, and CRF selectively excites glutamatergic projection neurons rather than GABAergic neurons in the cerebellar interpositus nucleus (IN) via two CRF receptors, CRFR1 and CRFR2, and their downstream inward rectifier K^+ channel and/or hyperpolarization-activated cyclic nucleotide-gated (HCN) channel. Furthermore, CRF promotes cerebellar motor coordination and rescues ataxic motor deficits. The findings define a previously unknown role for CRF in the olivo-cerebellar system in the control of gait, posture, and motor coordination, and provide new insight into the etiology, pathophysiology, and treatment strategy of cerebellar ataxia.

RESULTS

Downregulation of *Crf* mRNA in the Inferior Olive Induces Ataxia-like Motor Abnormalities

We found that corticotropin-releasing factor (CRF) and calbindin (a marker for inferior olive [IO] neurons [17]) were co-localized in neurons of all sub-nuclei in the IO (Figure S1), including the medial (IOM), principal (IOPr), and dorsal (IOD) nucleus (Figure 1A), which innervate the spinocerebellum. The result indicates an extensive distribution of CRFergic neurons in the IO.

To investigate the functional role of CRF in the IO, we downregulated *Crf* mRNA by *Crf*-RNAi-lentivirus (Figure 1B), which significantly decreased the level of *Crf* mRNA in the IO to 17.43% ± 0.01% ($p < 0.001$; Figure 1C). We employed footprint tests [18] to determine the effect of downregulation of *Crf* mRNA in the IO on locomotor gait. Lentivirus (LV)-*Crf*-RNAi treatment significantly shortened stride lengths ($n = 10$; left stride length: $p < 0.001$; right stride length: $p < 0.001$) and lengthened stride width ($n = 10$, $p < 0.05$) (Figure 1D). We also applied rota-rod and balance beam tests [19–21] to examine the effect of downregulation of *Crf* mRNA in the IO on motor coordination and balance. Rats treated with LV-*Crf*-RNAi displayed a remarkable decrease in the time spent on the accelerating rota-rod ($n = 10$, $p < 0.001$) (Figure 1E) and a prolonged time traversing the balance beam ($n = 11$, $p < 0.001$) (Figure 1F). These results strongly suggest that deficiency of CRF in the IO may result in cerebellar ataxia-like motor abnormalities, including gait disturbance, motor incoordination, and postural imbalance.

CRFergic Neurons in the IO Directly Project to the Cerebellar IN

Next, we microinjected the retrograde tracer Fluoro-Gold (Fluorochrome) into the cerebellar interpositus nucleus (IN) (Figure 2B), one of the two final output nodes of the spinocerebellum, for precise control of distal muscles of the limbs and digits [22–25]. We observed that the retrogradely labeled contralateral IO neurons also showed CRF immunoreactivity (Figure 2A), indicating direct CRFergic projections from the IO to the contralateral cerebellar IN. Fluoro-Gold-immunopositive fibers were also found in the inferior cerebellar peduncle (Figure 2C), through which the climbing fibers enter the cerebellum [26].

Both CRF Receptors Are Selectively Expressed and Co-localized in the Glutamatergic Neurons in the Cerebellar IN

We employed quantitative real-time RT-PCR and double immunostaining to assess the expression and distribution of two CRF receptors in the IN. The results showed that both *Crfr1* and *Crfr2* mRNAs were expressed in the IN (Figure 2D), and CRFR1 and CRFR2 (Figure 2E) were co-localized in the same IN neurons.

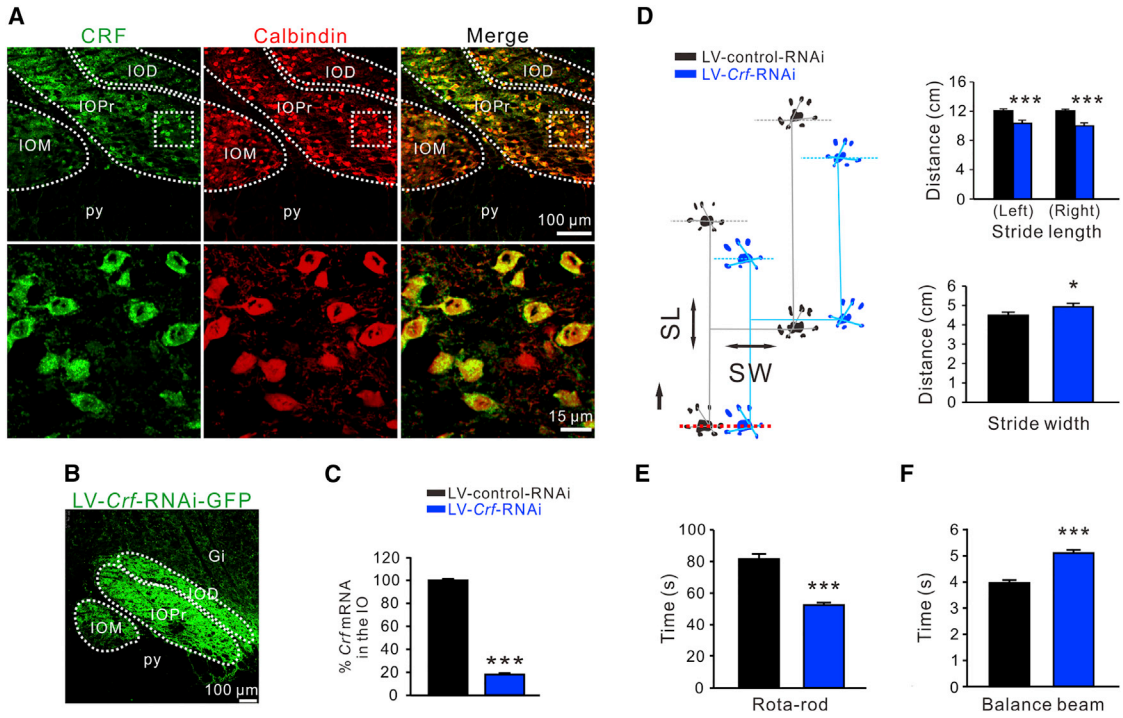

Figure 1. Downregulation of *Crf* mRNA in the IO Induces Ataxia-like Motor Abnormalities

(A) Double-immunostaining results showing that CRF was expressed in the calbindin-positive neurons in the IO. Gi, gigantocellular reticular nucleus; IOD, inferior olive dorsal nucleus; IOM, inferior olive medial nucleus; IOPr, inferior olive principal nucleus; py, pyramidal tract. Bottom: magnification of dotted squares (top).

(B) A brainstem slice showing the expression of microinjected LV-*Crf*-RNAi-GFP in the IO.

(C) Bar graphs showing the relative expression of *Crf* mRNA levels in the IO 21 days after injection of LV-*Crf*-RNAi or LV-control-RNAi (n = 6).

(D) Footprints of the hind paws of rats treated with LV-control-RNAi or LV-*Crf*-RNAi. Compared with the LV-control-RNAi group (n = 10), the LV-*Crf*-RNAi-treated rats showed abnormal gait, with shorter bilateral stride lengths (SLs) and a longer stride width (SW) (n = 10).

(E) The LV-*Crf*-RNAi-treated rats (n = 10) showed less endurance time on an accelerating rota-rod compared with the LV-control-RNAi group (n = 16).

(F) The LV-*Crf*-RNAi-treated rats (n = 11) exhibited a prolonged time traversing the balance beam compared with the LV-control-RNAi group (n = 13).

Data represent mean ± SEM; *p < 0.05 and ***p < 0.001, by unpaired two-tailed Student's t test (C–F). See also Figure S1.

Moreover, it has been well known that the IN contains glutamatergic, GABAergic, and GABA/glycinergic neurons [20, 27–29]. Interestingly, we found that CRFR2 was only localized in glutamate-immunopositive neurons (Figure 2F) rather than glutamate acid decarboxylase 67 (GAD67)-immunopositive ones (Figure 2G), suggesting that both CRF receptors are specifically co-expressed in the glutamatergic neurons but not the GABAergic or GABA/glycinergic neurons in the IN. Furthermore, it could be observed that the glutamatergic neurons expressing CRFR2 were large sized but the unexpressed CRFR2 neurons were small sized, and thus we speculated that CRF receptors are most likely to be expressed only in glutamatergic projection neurons and CRF may have a selective effect on IN projection neurons.

CRF Selectively Excites the Glutamatergic Projection Neurons in the IN and Promotes Motor Performance via CRFR1 and CRFR2

Using whole-cell patch-clamp recordings on cerebellar slices, we identified 60 projection neurons (Figure 3A) and 6 interneurons (Figure 3B) among the total of 66 recorded spontaneously active neurons in the IN by their electrophysiological and morphological properties [20, 27–29]. Notably, we found that CRF induced a significant inward current on most of the recorded projection neurons (58/60, 96.7%) but had no effect on interneurons (0/6, 0%), strongly suggesting a selective excitatory effect of CRF on projection neurons rather than interneurons in the cerebellar IN (Figures 3A and 3B). Accordingly, CRF remarkably increased the firing rate of IN projection neurons (Figures S2A and S2B) and elicited an inward current in a concentration-dependent manner (n = 6; Figures S2C and S2D). Given the above immunostaining results that CRF receptors were specifically expressed in the glutamatergic neurons, the projection neurons of the IN, we suggest that CRF may selectively modulate the glutamatergic projection neurons in the cerebellar IN.

Next, we examined the receptor mechanisms underlying the excitation of CRF on IN projection neurons. Co-application of tetrodotoxin (TTX), 2,3-dioxo-6-nitro-1,2,3,4-tetrahydrobenzo[f] quinoxaline-7-sulfonamide (NBQX), D-(-)-2-amino-5-phosphonopentanoic acid (D-AP5), and gabazine did not block the CRF-elicited inward currents on the recorded neurons (n = 5, p = 0.362; Figures 3C and 3D), indicating a direct postsynaptic effect of CRF. Moreover, the CRF-induced inward currents were partly antagonized by antalarmin (selective CRFR1 antagonist; n = 5, p < 0.01) or antisauvagine-30 (aSVG-30; selective CRFR2 antagonist; n = 6, p < 0.01), and nearly totally blocked

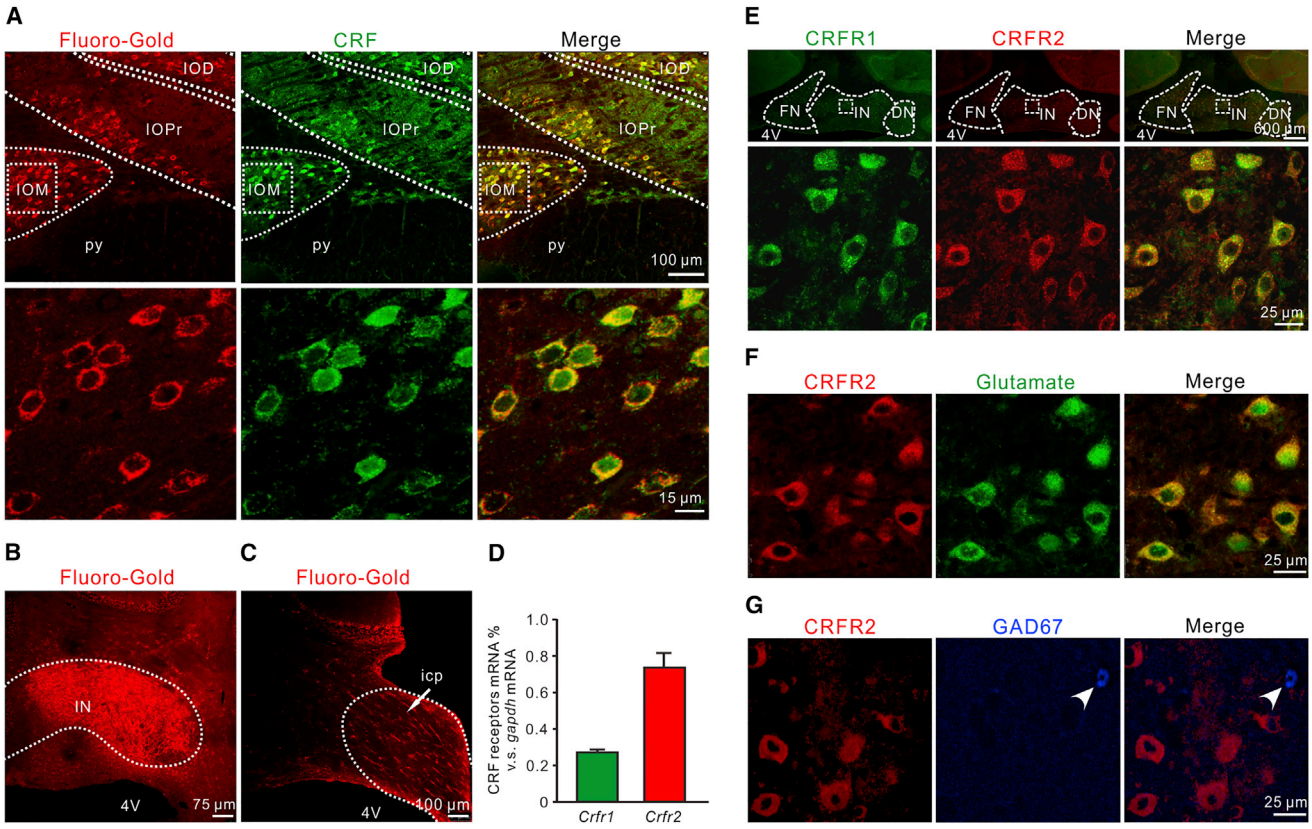

Figure 2. CRFergic Neurons in the IO Directly Project to the Cerebellar IN, and CRFR1 and CRFR2 Are Co-expressed in the Cerebellar IN Glutamatergic Neurons

(A) Retrograde tracer Fluoro-Gold and CRF were co-localized in neurons in the contralateral IO. Bottom: magnification of dotted squares (top). IOD, inferior olive dorsal nucleus; IOM, inferior olive medial nucleus; IOPr, inferior olive principal nucleus; py, pyramidal tract.

(B) A cerebellar slice showing the injection site of Fluoro-Gold. IN, interpositus nucleus; 4V, 4th ventricle.

(C) Fluoro-Gold-labeled fibers were observed in the inferior cerebellar peduncle. icp, inferior cerebellar peduncle.

(D) Bar graphs showing the relative expression of *Crfr1* and *Crfr2* mRNAs to *gapdh* mRNA in the cerebellar IN (n = 6). Data represent mean ± SEM.

(E) Double-immunostaining results showing that two CRF receptors, CRFR1 and CRFR2, were not only present in the cerebellar IN but also co-localized in the same IN neurons. DN, dentate nucleus; FN, fastigial nucleus; IN, interpositus nucleus. Bottom: magnification of dotted squares (top).

(F and G) CRFR2 was co-localized with glutamate (F) rather than GAD67 (G), a key enzyme in GABA biosynthesis, in IN neurons, indicating a selective expression of CRF receptors in glutamatergic rather than GABAergic neurons in the cerebellar IN. White arrowheads indicate a GAD67-positive neuron that did not express CRFR2.

by combined application of antalarmin and aSVG-30 (n = 6, $p < 0.001$) (Figures 3E and 3F), suggesting that both CRFR1 and CRFR2 are involved in the CRF-induced excitation on IN projection neurons.

We used selective agonists for CRFR1 (stressin-I) and CRFR2 (urocortin-II; UCN-II) to further determine the ionic mechanisms separately coupled to CRFR1 and CRFR2. The outwardly rectifying properties of the stressin-I-induced K^+ current (Figure S3A) and the hypopolarization-activated current increased by stressin-I (Figures S3B, S3D, and S3E), together with the stressin-I-enhanced voltage sag (Figures S3F and S3G), imply a dual ionic mechanism involving both the inward rectifier K^+ channel and the HCN channel. In addition, the stressin-I-elicited inward currents were partly blocked by ZD7288 (selective blocker for HCN channel; n = 6, $p < 0.01$) or tertiapin-Q (selective blocker for inward rectifier K^+ channel; n = 6, $p < 0.01$), and nearly totally antagonized by co-application of ZD7288 and tertiapin-Q (n = 6, $p < 0.001$) (Figures 3G and 3H). These results suggest that closure of the inward rectifier K^+ channel and activation of the HCN channel co-mediate the excitatory effect of CRFR1 activation on IN projection neurons.

On the other hand, the UCN-II-induced inward currents also showed outward rectification and reversed at the calculated E_k potential of −105 mV (Figure S4). Tertiapin-Q totally blocked the inward currents induced by UCN-II (n = 6, $p < 0.001$; Figures 3I and 3J), indicating an involvement of the inward rectifier K^+ channel in the excitation induced by activation of CRFR2. Furthermore, the CRF-induced inward currents were totally antagonized by co-application of ZD7288 and tertiapin-Q (n = 5, $p < 0.001$; Figures 3K and 3L), confirming that both the inward rectifier K^+ channel coupled to CRFR1 and CRFR2 and the HCN channel linked to CRFR1 contribute to the excitatory effect of CRF on projection neurons in the cerebellar IN.

Therefore, the issue was raised whether the effect of CRF on the glutamatergic projection neurons in the IN could consequently modulate cerebellar motor control. We found that

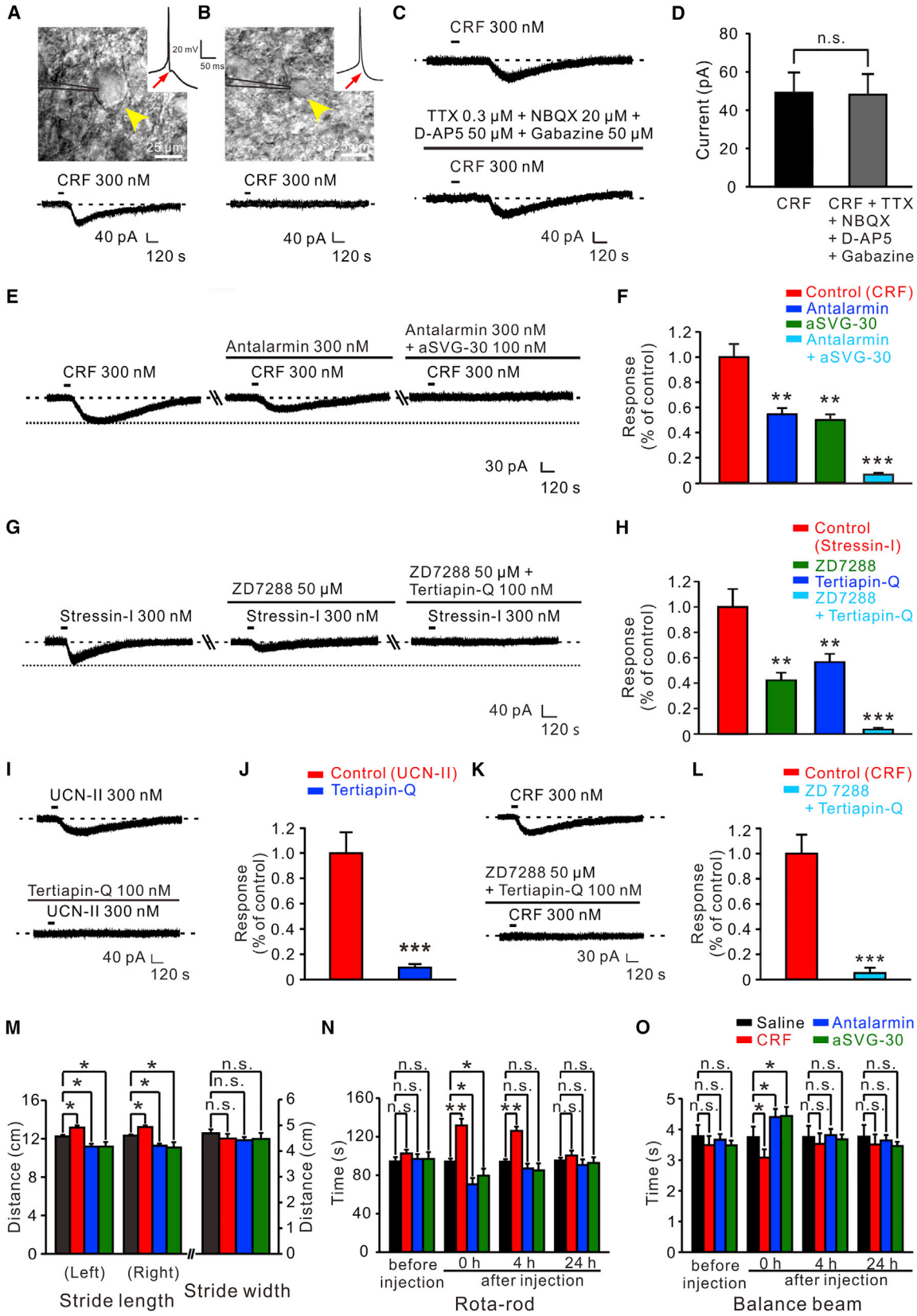

(legend on next page)

microinjection of CRF into bilateral INs in normal rats significantly enlarged stride lengths (n = 9; left: $p < 0.05$; right: $p < 0.05$), whereas blockage of CRFR1 or CRFR2 by antalarmin (n = 10; left: $p < 0.05$; right: $p < 0.05$) or aSVG-30 (n = 9; left: $p < 0.05$; right: $p < 0.05$) remarkably shortened stride lengths (Figure 3M). However, CRF did not influence stride width (Figure 3M), which is consistent with the function of the IN in modulation on more distal musculature [30, 31]. In addition, CRF significantly improved motor performance of normal rats on the accelerating rota-rod (n = 11, $p < 0.01$) and balance beam (n = 9, $p < 0.05$), whereas antalarmin (rota-rod: n = 10, $p < 0.05$; balance beam: n = 9, $p < 0.05$) or aSVG-30 (rota-rod: n = 10, $p < 0.05$; balance beam: n = 9, $p < 0.05$) attenuated motor performance (Figures 3N and 3O). These results suggest that CRF may promote motor coordination and motor balance through the mediation of the inward rectifier K^+ channel and/or HCN channel coupled to CRFR1 and CRFR2 in the IN, and endogenous CRFergic afferent inputs may participate in cerebellar motor control via their direct modulation on the glutamatergic projection neurons in the cerebellar nuclei.

CRF Rescues Cerebellar Ataxia-like Motor Abnormalities

To examine the role of CRFergic modulation in the IN in cerebellar ataxic motor disorders, we first tested the level of CRF in the IN following downregulation of *Crf* mRNA in the IO and found it was significantly decreased (Figure 4A). As expected, microinjection of CRF into bilateral INs remarkably ameliorated stride lengths of LV-*Crf*-RNAi-treated rats (n = 10; left: $p < 0.01$; right: $p < 0.001$) (Figure 4B). CRF also markedly alleviated motor incoordination and imbalance of the ataxia-like rats on the rota-rod (n = 13, $p < 0.001$; Figure 4C) and balance beam (n = 13, $p < 0.001$; Figure 4D). These results indicate that the ataxia-like motor dysfunction caused by deficiency of CRF in the IO may be ameliorated by elevation of CRF level in the cerebellar IN.

We also made a rat model of cerebellar ataxia by intraperitoneal injection of 3-acetylpyridine (3-AP), a neurotoxin that selectively destroys IO neurons [32, 33]. As shown in Figure 4E, 3-AP caused a significant loss of calbindin-immunopositive neurons in the IO, including the CRFergic neurons. The 3-AP-treated rats presented severe ataxia-like motor abnormalities, including gait disturbance (n = 9; left: $p < 0.05$; right: $p < 0.05$; Figure 4F) and motor incoordination on the rota-rod (n = 9, $p < 0.001$; Figure 4G) and balance beam (n = 11, $p < 0.001$; Figure 4H). Microinjection of CRF into bilateral INs significantly ameliorated the stride lengths in gait disturbance (n = 9; left: $p < 0.05$; right: $p < 0.05$; Figure 4F) as well as motor incoordination and imbalance (rota-rod: n = 11, $p < 0.001$; balance beam: n = 12, $p < 0.001$; Figures 4G and 4H). These results strongly suggest that the CRF in the olivo-cerebellar system may hold a key position in cerebellar ataxia.

DISCUSSION

CRF is a hormone and neurotransmitter mainly synthesized in the hypothalamic paraventricular nucleus, and has traditionally been implicated in stress and anxiety [8, 34, 35]. Here we demonstrate that the CRF in the olivo-cerebellar system plays an essential functional role in cerebellar motor control and ataxia via its direct modulation on the glutamatergic projection neurons in cerebellar nuclei.

The IO has been implicated not only in motor learning but also in controlling ongoing movement [36–40]. Lesion of the IO causes ataxic and dysmetric motor abnormalities including gait disturbance and motor incoordination [41, 42], and abnormal CRF levels in the IO were reported in ataxic patients and mutant animals [15, 16, 43, 44], indicating a close relationship between the olivo-cerebellar CRFergic system and cerebellar ataxia. In the present study, we find that both downregulation of *Crf*

Figure 3. CRF Selectively Excites the Projection Neurons in the Cerebellar IN and Promotes Motor Performance via the Co-mediation of CRFR1 and CRFR2

(A) CRF elicited an inward current in a recorded projection neuron in the cerebellar IN. Neurons with diameter larger than 20 μm (indicated by the yellow arrowhead) and a complex waveform of action potential (indicated by the red arrow) were identified as projection neurons.

(B) CRF had no effect on a recorded interneuron in the cerebellar IN. Neurons with diameter less than 10 μm (indicated by the yellow arrowhead) and a simple waveform of action potential (indicated by the red arrow) were categorized as interneurons.

(C) TTX combined with NBQX, D-AP5, and gabazine did not influence the CRF-induced inward current in a recorded IN projection neuron.

(D) Group data of the tested neurons (n = 5; p = 0.362).

(E) The CRF-induced inward current in a recorded neuron was partly blocked by antalarmin (selective CRFR1 antagonist) and totally abolished by combined application of antalarmin and aSVG-30 (selective CRFR2 antagonist).

(F) Group data of the tested neurons (n = 5 for antalarmin; n = 6 for separate application of aSVG-30 or for combined application).

(G) The stressin-I-induced inward current in a recorded neuron was partly blocked by ZD7288 (selective blocker for HCN channel) and totally abolished by combined application of ZD7288 and tertiapin-Q (selective blocker for inward rectifier K^+ channel).

(H) Group data of the tested neurons (n = 6).

(I) The UCN-II-evoked current was antagonized by tertiapin-Q.

(J) Group data of the tested neurons (n = 6).

(K) The CRF-elicited current was totally blocked by co-application of ZD7288 and tertiapin-Q.

(L) Group data of the tested neurons (n = 5).

(M) Microinjection of CRF (n = 9) into the bilateral cerebellar INs significantly increased the bilateral stride lengths rather than stride width compared with the saline group (n = 11), whereas antalarmin (n = 10) or aSVG-30 (n = 9) remarkably shortened stride lengths, but not stride width.

(N) CRF significantly prolonged the endurance time of rats on the accelerating rota-rod (n = 11) compared with the saline group (n = 9), whereas antalarmin (n = 10) or aSVG-30 (n = 10) shortened the endurance time.

(O) CRF (n = 9) remarkably decreased time spent traversing the balance beam compared with the saline group (n = 9), whereas antalarmin (n = 9) or aSVG-30 (n = 9) increased the time to traverse the balance beam.

Data represent mean ± SEM; *$p < 0.05$, **$p < 0.01$, and ***$p < 0.001$, and n.s. indicates not significant, by paired two-tailed Student's t test (D, J, and L), or one-way (F and H) or repeated-measures two-way ANOVA (M–O) followed by Newman-Keuls post hoc test.

See also Figures S2–S4.

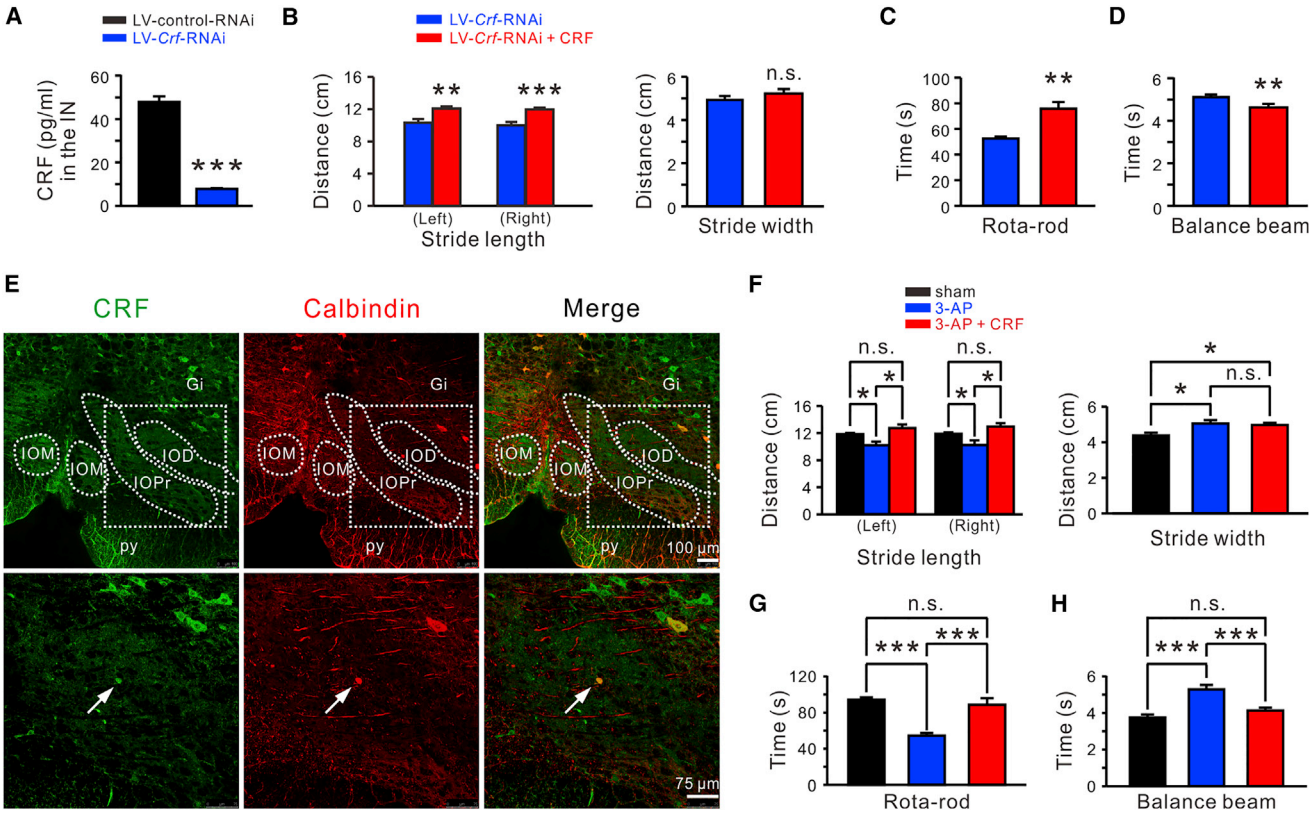

Figure 4. Microinjection of CRF into the Cerebellar INs Rescues Motor Abnormalities Caused by Downregulation of *Crf* mRNA in the IO or Intraperitoneal Injection of 3-AP

(A) Bar graphs showing the CRF level in the cerebellar IN detected by ELISA 21 days after injection of LV-*Crf*-RNAi or LV-control-RNAi into the IO.

(B) Microinjection of CRF into the bilateral INs restored the bilateral stride lengths rather than stride width in the LV-*Crf*-RNAi-treated rats (n = 10).

(C and D) Microinjection of CRF into the bilateral INs improved motor performance of the LV-*Crf*-RNAi-treated rats on the accelerating rota-rod (n = 13) (C) and balance beam (n = 13) (D).

(E) Double immunostainings showing the loss of CRF/calbindin-positive neurons 3 days after intraperitoneal injection of 3-AP. The white arrows show a surviving CRFergic neuron in the IO. Bottom: magnification of dotted squares (top).Gi, gigantocellular reticular nucleus; IOD, inferior olive dorsal nucleus; IOM, inferior olive medial nucleus; IOPr, inferior olive principal nucleus; py, pyramidal tract.

(F) 3-AP-induced ataxic rats (n = 9) showed shorter stride lengths and a longer stride width compared with the sham group (n = 11). Microinjection of CRF into bilateral INs of ataxic rats (n = 9) significantly rescues stride lengths rather than stride width.

(G) The endurance time of 3-AP-treated rats (n = 9) on the rota-rod was significantly shorter than that of the sham group (n = 10). Microinjection of CRF into bilateral INs remarkably prolonged the endurance time of ataxic rats (n = 11).

(H) 3-AP-treated rats (n = 11) spent a longer time traversing the balance beam compared with the sham group (n = 11). CRF significantly reduced the time of ataxic rats (n = 12) traversing the beam.

Data represent mean ± SEM; *p < 0.05, **p < 0.01, and ***p < 0.001, and n.s. indicates not significant, by unpaired two-tailed Student's t test (A–D) or one-way ANOVA followed by Newman-Keuls post hoc test (F–H).

mRNA in the IO (Figure 1) and antagonization of CRF receptors (Figures 3M–3O) that block CRFergic afferent inputs in the IN induce ataxia-like gait abnormality, motor incoordination, and postural instability. On the contrary, microinjection of CRF into the IN enlarges stride lengths (Figure 3M) and ameliorates motor deficits (Figure 4), which is consistent with a previous study on cerebellar control of gait and interlimb coordination [45]. We therefore suggest that the olivo-cerebellar CRFergic system may greatly contribute to the cerebellar control of ongoing movement and is closely associated with the motor symptoms of cerebellar ataxia.

Although Olschowka et al. only identified a moderate number of CRF-like fibers in the cerebellum [46], accumulating studies have reported a substantial number of CRF-immunopositive fibers in the cerebellar cortex [10–13] and revealed a modulation of CRF on activity, synaptic transmission, plasticity, and differentiation of cerebellar Purkinje cells [47–51]. Intracerebroventricular injection of CRF can even enhance eye blink conditioning [52]. However, the physiological functions and mechanisms of CRF in cerebellar control of gait and motor coordination remain enigmatic. Climbing fibers originating from the IO project not only to the cerebellar cortex but also to the cerebellar nuclei [26, 53], which constitute the primary cerebellar circuits with mossy fiber collaterals to the cerebellar nuclei [54]. In the present study, we reveal, for the first time, that CRFergic neurons in the IO project directly into the cerebellar IN, one of the final integration and output nodes for the spinocerebellum, and CRF selectively excites the glutamatergic projection neurons rather than

GABAergic or GABA/glycinergic interneurons in the IN. It has been reported that climbing fibers from the ventrolateral outgrowth of the IO to the ventral dentate nucleus and vestibular nuclei also contact the GABAergic neurons, implying a different organization and regulation of CRFergic afferent inputs in the vestibulocerebellum [55, 56]. Because the glutamatergic neurons are the only principal neurons in the IN, whereas GABAergic and GABA/glycinergic neurons are nucleo-olivary feedback neurons or interneurons [20, 27–29], we propose that the selective excitation of CRF on glutamatergic projection neurons in the IN, via CRFR1 and CRFR2 and their downstream inward rectifier K^+ channel and/or HCN channel, will quickly regulate neuronal excitability, enhance the ultimate output of the spinocerebellum, and rapidly modulate motor coordination and balance in ongoing movements, without redundantly biasing the local circuit.

Ataxia is the most common motor disorder caused by cerebellar lesion. However, effective treatment for ataxic motor dysfunction is still lacking. In this study, microinjection of CRF into the cerebellar IN not only promoted the motor performance of normal rats but also significantly ameliorated gait disturbance, motor incoordination, and imbalance in both ataxic rat models with downregulation of CRF in the IO or treatment with 3-AP. Therefore, our results define an indispensable role for CRF in the olivo-cerebellar system in cerebellar motor coordination, and provide novel insight into the etiology, pathophysiology, and treatment strategy of cerebellar ataxia. The findings also contribute to understanding the function of the central CRF system in motor control and motor diseases.

STAR★METHODS

Detailed methods are provided in the online version of this paper and include the following:

- KEY RESOURCES TABLE
- CONTACT FOR REAGENT AND RESOURCE SHARING
- EXPERIMENTAL MODEL AND SUBJECT DETAILS
  - Rat
- METHOD DETAILS
  - Lentiviral transduction and stereotactic microinjection
  - Quantitative real-time RT-PCR
  - Retrograde tracings
  - Immunofluorescence
  - Stereotactic cannula placement and behavioral tests
  - Whole-cell patch clamp recordings on brain slices
  - Rat model of cerebellar ataxia
  - Histological identification
- QUANTIFICATION AND STATISTICAL ANALYSIS

SUPPLEMENTAL INFORMATION

Supplemental Information includes four figures and can be found with this article online at http://dx.doi.org/10.1016/j.cub.2017.07.035.

AUTHOR CONTRIBUTIONS

J.-N.Z. and J.-J.W. designed the research; Y.W., Z.-P.C., and Q.-X.Z. performed the research; Y.W., Z.-P.C., Q.-X.Z., X.-Y.Z., and H.-Z.L. analyzed the data; Y.W. and Z.-P.C. prepared the figures and manuscript draft; and J.-N.Z. and J.-J.W. wrote the paper.

ACKNOWLEDGMENTS

This work was supported by the National Natural Science Foundation of China (grants 81671107, 31330033, 91332124, 31471112, 31600834, and NSFC/RGC Joint Research Scheme 31461163001), the Ministry of Education of China (SRFDP/RGC ERG grant 20130091140003, NCET program, and Fundamental Research Funds for the Central Universities 020814380071), and the Natural Science Foundation of Jiangsu Province, China (grant BK20151384).

Received: May 26, 2017
Revised: July 11, 2017
Accepted: July 13, 2017
Published: August 24, 2017

REFERENCES

1. Manto, M. (2008). The cerebellum, cerebellar disorders, and cerebellar research—two centuries of discoveries. Cerebellum *7*, 505–516.
2. Durr, A. (2010). Autosomal dominant cerebellar ataxias: polyglutamine expansions and beyond. Lancet Neurol. *9*, 885–894.
3. Anheim, M., Tranchant, C., and Koenig, M. (2012). The autosomal recessive cerebellar ataxias. N. Engl. J. Med. *366*, 636–646.
4. Bowen, M.T., Peters, S.T., Absalom, N., Chebib, M., Neumann, I.D., and McGregor, I.S. (2015). Oxytocin prevents ethanol actions at δ subunit-containing GABAA receptors and attenuates ethanol-induced motor impairment in rats. Proc. Natl. Acad. Sci. USA *112*, 3104–3109.
5. Ito, H., Fujita, K., Tagawa, K., Chen, X., Homma, H., Sasabe, T., Shimizu, J., Shimizu, S., Tamura, T., Muramatsu, S., and Okazawa, H. (2015). HMGB1 facilitates repair of mitochondrial DNA damage and extends the lifespan of mutant ataxin-1 knock-in mice. EMBO Mol. Med. *7*, 78–101.
6. Zhou, L., Yang, D., Wang, D.J., Xie, Y.J., Zhou, J.H., Zhou, L., Huang, H., Han, S., Shao, C.Y., Li, H.S., et al. (2015). Numb deficiency in cerebellar Purkinje cells impairs synaptic expression of metabotropic glutamate receptor and motor coordination. Proc. Natl. Acad. Sci. USA *112*, 15474–15479.
7. Hoch, N.C., Hanzlikova, H., Rulten, S.L., Tétreault, M., Komulainen, E., Ju, L., Hornyak, P., Zeng, Z., Gittens, W., Rey, S.A., et al.; Care4Rare Canada Consortium (2017). XRCC1 mutation is associated with PARP1 hyperactivation and cerebellar ataxia. Nature *541*, 87–91.
8. Vale, W., Spiess, J., Rivier, C., and Rivier, J. (1981). Characterization of a 41-residue ovine hypothalamic peptide that stimulates secretion of corticotropin and beta-endorphin. Science *213*, 1394–1397.
9. Hauger, R.L., Risbrough, V., Brauns, O., and Dautzenberg, F.M. (2006). Corticotropin releasing factor (CRF) receptor signaling in the central nervous system: new molecular targets. CNS Neurol. Disord. Drug Targets *5*, 453–479.
10. Cummings, S., Elde, R., Ells, J., and Lindall, A. (1983). Corticotropin-releasing factor immunoreactivity is widely distributed within the central nervous system of the rat: an immunohistochemical study. J. Neurosci. *3*, 1355–1368.
11. Palkovits, M., Léránth, C., Görcs, T., and Young, W.S., III. (1987). Corticotropin-releasing factor in the olivocerebellar tract of rats: demonstration by light- and electron-microscopic immunohistochemistry and in situ hybridization histochemistry. Proc. Natl. Acad. Sci. USA *84*, 3911–3915.
12. Sakanaka, M., Shibasaki, T., and Lederis, K. (1987). Corticotropin releasing factor-like immunoreactivity in the rat brain as revealed by a modified cobalt-glucose oxidase-diaminobenzidine method. J. Comp. Neurol. *260*, 256–298.
13. Cummings, S., Sharp, B., and Elde, R. (1988). Corticotropin-releasing factor in cerebellar afferent systems: a combined immunohistochemistry and retrograde transport study. J. Neurosci. *8*, 543–554.
14. Ito, M. (2009). Functional roles of neuropeptides in cerebellar circuits. Neuroscience *162*, 666–672.

15. Suemaru, S., Suemaru, K., Kawai, K., Miyata, S., Nobukuni, K., Ihara, Y., Namba, R., Urakami, K., and Hashimoto, K. (1995). Cerebrospinal fluid corticotropin-releasing hormone in neurodegenerative diseases: reduction in spinocerebellar degeneration. Life Sci. *57*, 2231–2235.
16. Mizuno, Y., Takahashi, K., Totsune, K., Ohneda, M., Konno, H., Murakami, O., Satoh, F., Sone, M., Takase, S., Itoyama, Y., et al. (1995). Decrease in cerebellin and corticotropin-releasing hormone in the cerebellum of olivopontocerebellar atrophy and Shy-Drager syndrome. Brain Res. *686*, 115–118.
17. Airaksinen, M.S., Eilers, J., Garaschuk, O., Thoenen, H., Konnerth, A., and Meyer, M. (1997). Ataxia and altered dendritic calcium signaling in mice carrying a targeted null mutation of the calbindin D28k gene. Proc. Natl. Acad. Sci. USA *94*, 1488–1493.
18. He, Y.C., Wu, G.Y., Li, D., Tang, B., Li, B., Ding, Y., Zhu, J.N., and Wang, J.J. (2012). Histamine promotes rat motor performances by activation of H(2) receptors in the cerebellar fastigial nucleus. Behav. Brain Res. *228*, 44–52.
19. Zhang, J., Li, B., Yu, L., He, Y.C., Li, H.Z., Zhu, J.N., and Wang, J.J. (2011). A role for orexin in central vestibular motor control. Neuron *69*, 793–804.
20. Zhang, J., Zhuang, Q.X., Li, B., Wu, G.Y., Yung, W.H., Zhu, J.N., and Wang, J.J. (2016). Selective modulation of histaminergic inputs on projection neurons of cerebellum rapidly promotes motor coordination via HCN channels. Mol. Neurobiol. *53*, 1386–1401.
21. Li, B., Zhang, X.Y., Yang, A.H., Peng, X.C., Chen, Z.P., Zhou, J.Y., Chan, Y.S., Wang, J.J., and Zhu, J.N. (2017). Histamine increases neuronal excitability and sensitivity of the lateral vestibular nucleus and promotes motor behaviors via HCN channel coupled to H2 receptor. Front. Cell. Neurosci. *10*, 300.
22. Ito, M. (2006). Cerebellar circuitry as a neuronal machine. Prog. Neurobiol. *78*, 272–303.
23. Hoebeek, F.E., Witter, L., Ruigrok, T.J., and De Zeeuw, C.I. (2010). Differential olivo-cerebellar cortical control of rebound activity in the cerebellar nuclei. Proc. Natl. Acad. Sci. USA *107*, 8410–8415.
24. Perciavalle, V., Apps, R., Bracha, V., Delgado-García, J.M., Gibson, A.R., Leggio, M., Carrel, A.J., Cerminara, N., Coco, M., Gruart, A., and Sánchez-Campusano, R. (2013). Consensus paper: current views on the role of cerebellar interpositus nucleus in movement control and emotion. Cerebellum *12*, 738–757.
25. Song, Y.N., Li, H.Z., Zhu, J.N., Guo, C.L., and Wang, J.J. (2006). Histamine improves rat rota-rod and balance beam performances through H(2) receptors in the cerebellar interpositus nucleus. Neuroscience *140*, 33–43.
26. Sugihara, I., Wu, H., and Shinoda, Y. (1999). Morphology of single olivocerebellar axons labeled with biotinylated dextran amine in the rat. J. Comp. Neurol. *414*, 131–148.
27. Aizenman, C.D., Huang, E.J., and Linden, D.J. (2003). Morphological correlates of intrinsic electrical excitability in neurons of the deep cerebellar nuclei. J. Neurophysiol. *89*, 1738–1747.
28. Uusisaari, M., Obata, K., and Knöpfel, T. (2007). Morphological and electrophysiological properties of GABAergic and non-GABAergic cells in the deep cerebellar nuclei. J. Neurophysiol. *97*, 901–911.
29. Bagnall, M.W., Zingg, B., Sakatos, A., Moghadam, S.H., Zeilhofer, H.U., and du Lac, S. (2009). Glycinergic projection neurons of the cerebellum. J. Neurosci. *29*, 10104–10110.
30. Ilg, W., Giese, M.A., Gizewski, E.R., Schoch, B., and Timmann, D. (2008). The influence of focal cerebellar lesions on the control and adaptation of gait. Brain *131*, 2913–2927.
31. Dimitrova, A., de Greiff, A., Schoch, B., Gerwig, M., Frings, M., Gizewski, E.R., and Timmann, D. (2006). Activation of cerebellar nuclei comparing finger, foot and tongue movements as revealed by fMRI. Brain Res. Bull. *71*, 233–241.
32. O'Hearn, E., and Molliver, M.E. (1997). The olivocerebellar projection mediates ibogaine-induced degeneration of Purkinje cells: a model of indirect, trans-synaptic excitotoxicity. J. Neurosci. *17*, 8828–8841.
33. Fernandez, A.M., de la Vega, A.G., and Torres-Aleman, I. (1998). Insulin-like growth factor I restores motor coordination in a rat model of cerebellar ataxia. Proc. Natl. Acad. Sci. USA *95*, 1253–1258.
34. Bale, T.L., and Vale, W.W. (2004). CRF and CRF receptors: role in stress responsivity and other behaviors. Annu. Rev. Pharmacol. Toxicol. *44*, 525–557.
35. de Kloet, E.R., Joëls, M., and Holsboer, F. (2005). Stress and the brain: from adaptation to disease. Nat. Rev. Neurosci. *6*, 463–475.
36. Llinás, R.R. (2014). The olivo-cerebellar system: a key to understanding the functional significance of intrinsic oscillatory brain properties. Front. Neural Circuits *7*, 96.
37. Welsh, J.P., Lang, E.J., Suglhara, I., and Llinás, R. (1995). Dynamic organization of motor control within the olivocerebellar system. Nature *374*, 453–457.
38. Llinás, R., Walton, K., Hillman, D.E., and Sotelo, C. (1975). Inferior olive: its role in motor learing. Science *190*, 1230–1231.
39. Lang, E.J., Apps, R., Bengtsson, F., Cerminara, N.L., De Zeeuw, C.I., Ebner, T.J., Heck, D.H., Jaeger, D., Jörntell, H., Kawato, M., et al. (2017). The roles of the olivocerebellar pathway in motor learning and motor control. A consensus paper. Cerebellum *16*, 230–252.
40. De Zeeuw, C.I., and Ten Brinke, M.M. (2015). Motor learning and the cerebellum. Cold Spring Harb. Perspect. Biol. *7*, a021683.
41. Seoane, A., Apps, R., Balbuena, E., Herrero, L., and Llorens, J. (2005). Differential effects of *trans*-crotononitrile and 3-acetylpyridine on inferior olive integrity and behavioural performance in the rat. Eur. J. Neurosci. *22*, 880–894.
42. Horn, K.M., Deep, A., and Gibson, A.R. (2013). Progressive limb ataxia following inferior olive lesions. J. Physiol. *591*, 5475–5489.
43. Sawada, K., Kawano, M., Tsuji, H., Sakata-Haga, H., Hisano, S., and Fukui, Y. (2003). Over-expression of corticotropin-releasing factor mRNA in inferior olivary neurons of rolling mouse Nagoya. Brain Res. Mol. Brain Res. *117*, 190–195.
44. Jeong, Y.G., Chung, S.H., Kim, C.T., Kim, K.H., Han, S.Y., Hyun, B.H., Lee, N.S., Sawada, K., Won, M.H., and Fukui, Y. (2006). Corticotropin-releasing factor immunoreactivity increases in the cerebellar climbing fibers in the novel ataxic mutant mouse, pogo. Anat. Histol. Embryol. *35*, 111–115.
45. Vinueza Veloz, M.F., Zhou, K., Bosman, L.W., Potters, J.W., Negrello, M., Seepers, R.M., Strydis, C., Koekkoek, S.K., and De Zeeuw, C.I. (2015). Cerebellar control of gait and interlimb coordination. Brain Struct. Funct. *220*, 3513–3536.
46. Olschowka, J.A., O'Donohue, T.L., Mueller, G.P., and Jacobowitz, D.M. (1982). The distribution of corticotropin releasing factor-like immunoreactive neurons in rat brain. Peptides *3*, 995–1015.
47. Bishop, G.A. (1990). Neuromodulatory effects of corticotropin releasing factor on cerebellar Purkinje cells: an in vivo study in the cat. Neuroscience *39*, 251–257.
48. Miyata, M., Okada, D., Hashimoto, K., Kano, M., and Ito, M. (1999). Corticotropin-releasing factor plays a permissive role in cerebellar long-term depression. Neuron *22*, 763–775.
49. Schmolesky, M.T., De Ruiter, M.M., De Zeeuw, C.I., and Hansel, C. (2007). The neuropeptide corticotropin-releasing factor regulates excitatory transmission and plasticity at the climbing fibre-Purkinje cell synapse. Eur. J. Neurosci. *25*, 1460–1466.
50. Libster, A.M., Title, B., and Yarom, Y. (2015). Corticotropin-releasing factor increases Purkinje neuron excitability by modulating sodium, potassium, and Ih currents. J. Neurophysiol. *114*, 3339–3350.
51. Swinny, J.D., Metzger, F., Ijkema-Paassen, J., Gounko, N.V., Gramsbergen, A., and van der Want, J.J. (2004). Corticotropin-releasing factor and urocortin differentially modulate rat Purkinje cell dendritic outgrowth and differentiation in vitro. Eur. J. Neurosci. *19*, 1749–1758.
52. Servatius, R.J., Beck, K.D., Moldow, R.L., Salameh, G., Tumminello, T.P., and Short, K.R. (2005). A stress-induced anxious state in male rats: corticotropin-releasing hormone induces persistent changes in associative learning and startle reactivity. Biol. Psychiatry *57*, 865–872.

53. Pijpers, A., Voogd, J., and Ruigrok, T.J. (2005). Topography of olivo-cortico-nuclear modules in the intermediate cerebellum of the rat. J. Comp. Neurol. *492*, 193–213.

54. Shinoda, Y., Sugiuchi, Y., Futami, T., and Izawa, R. (1992). Axon collaterals of mossy fibers from the pontine nucleus in the cerebellar dentate nucleus. J. Neurophysiol. *67*, 547–560.

55. De Zeeuw, C.I., Gerrits, N.M., Voogd, J., Leonard, C.S., and Simpson, J.I. (1994). The rostral dorsal cap and ventrolateral outgrowth of the rabbit inferior olive receive a GABAergic input from dorsal group Y and the ventral dentate nucleus. J. Comp. Neurol. *341*, 420–432.

56. De Zeeuw, C.I., Van Alphen, A.M., Hawkins, R.K., and Ruigrok, T.J. (1997). Climbing fibre collaterals contact neurons in the cerebellar nuclei that provide a GABAergic feedback to the inferior olive. Neuroscience *80*, 981–986.

57. Paxinos, G., and Watson, C. (2007). The Rat Brain in Stereotaxic Coordinates, Sixth Edition (Academic Press/Elsevier).

58. Li, B., Zhuang, Q.X., Gao, H.R., Wang, J.J., and Zhu, J.N. (2017). Medial cerebellar nucleus projects to feeding-related neurons in the ventromedial hypothalamic nucleus in rats. Brain Struct. Funct. *222*, 957–971.

59. Zhang, C.Z., Zhuang, Q.X., He, Y.C., Li, G.Y., Zhu, J.N., and Wang, J.J. (2014). 5-HT2A receptor-mediated excitation on cerebellar fastigial nucleus neurons and promotion of motor behaviors in rats. Pflugers Arch. *466*, 1259–1271.

60. Zhang, X.Y., Yu, L., Zhuang, Q.X., Peng, S.Y., Zhu, J.N., and Wang, J.J. (2013). Postsynaptic mechanisms underlying the excitatory action of histamine on medial vestibular nucleus neurons in rats. Br. J. Pharmacol. *170*, 156–169.

STAR★METHODS

KEY RESOURCES TABLE

REAGENT or RESOURCE	SOURCE	IDENTIFIER
Antibodies		
Goat anti-CRF	Santa Cruz	Cat#SC-1759; RRID: AB_631300
Rabbit anti-calbindin	Millipore	Cat#PC253L; RRID: AB_213554
Rabbit anti-Fluoro-Gold	Millipore	Cat#AB153-I; RRID: AB_2632408
Goat anti-CRFR1	Abcam	Cat#ab59023; RRID: AB_941167
Rabbit anti-CRFR2	Abcam	Cat#ab75168; RRID: AB_1523392
Mouse anti-glutamate	Millipore	Cat#MAB5304; RRID: AB_94688
Mouse anti-GAD67	Millipore	Cat#MAB5406; RRID: AB_2278725
Bacterial and Virus Strains		
lentiviral vector GV118 (U6-MCS-Ubi-EGFP)	Genechem	N/A
Chemicals, Peptides, and Recombinant Proteins		
Fluoro-gold	Fluorochrome	Cat#52-9400
Corticotropin-releasing factor	Millipore	Cat#05-23-0050
Tetrodotoxin	Alomone Labs	Cat#T-500
D-AP5	Tocris	Cat#0106
NBQX	Tocris	Cat#1044
Gabazine	Tocris	Cat#1262
Antalarmin	Tocris	Cat#2778
Antisauvagine-30	Tocris	Cat#2071
Stressin-I	Tocirs	Cat#1608
Urocortin-II	Phoenix	Cat#019-34
ZD2788	Tocris	Cat#1000
Tertiapin-Q	Tocris	Cat#1316
3-acetylpyridine	Sigma-Aldrich	Cat#04642
Critical Commercial Assays		
Fluoromount-G mounting medium	SouthernBiotech	Cat#010020
TriZol reagent	Invitrogen	Cat#15596-018
M-MLV reverse transcriptase	Promega	Cat#M1701
iQ SYBR Green SuperMix	Bio-Rad	Cat#1708887
CRF ELISA Mouse/Rat kit	Biovendor	Cat#RSCYK131R
Experimental Models: Organisms/Strains		
Rat: Sprague-Dawley	Experimental Animal Center of Nanjing Medical University	N/A
Oligonucleotides		
Primers for *Crf*: F, 5′-TGA TCC GCA TGG GTG AAG AA TAC TTC CTC-3′; R, 5′-CCC GAT AAT CTC CAT CAG TTT CCT GTT GCT G-3′	This paper	N/A
Primers for *Crfr1*: F, 5′-TGC CTG AGA AAC ATC ATC CAC TGG-3′; R, 5′-TAA TTG TAG GCG GCT GTC ACC AAC-3′	This paper	N/A
Primers for *Crfr2*: F, 5′-AAC GGC ATC AAG TAC AAC ACG AC-3′; R, 5′-CG ATT CGG TAA TGC AGG TCA TAC-3′	This paper	N/A
Primers for *gapdh*: F, 5′-GGT GCT GAG TAT GTC GTG GAG TCT AC-3′; R, 5′-CAT GTA GGC CAT GAG GTC CAC CAC C-3′	This paper	N/A

(*Continued on next page*)

Continued

REAGENT or RESOURCE	SOURCE	IDENTIFIER
Recombinant DNA		
LV-*Crf*-RNAi (sequence for *Crf* was 5′- AGA TTA TCG GGA AAT GAA A-3′)	This paper	N/A
LV-control-RNAi (sequence for the control siRNA was 5′-TTC TCC GAA CGT GTC ACG T-3′)	This paper	N/A
Software and Algorithms		
SigmaPlot 12.5	Systat Software	https://systatsoftware.com/products/sigmaplot/
SPSS 22	SPSS	https://www.ibm.com/analytics/us/en/technology/spss/

CONTACT FOR REAGENT AND RESOURCE SHARING

Further information and requests for resources and reagents should be directed to and will be fulfilled by the Lead Contact, Jing-Ning Zhu (jnzhu@nju.edu.cn).

EXPERIMENTAL MODEL AND SUBJECT DETAILS

Rat

Adult male Sprague-Dawley rats (Experimental Animal Center of Nanjing Medical University, Nanjing, China) were used in behavioral, tracing, RT-PCR, and immnostaining experiments. Rats aged 12-18 days of either sex were used in patch clamp recordings on brain slices. Rats were individually housed under controlled environmental conditions (24 ± 2°C; 60 ± 5% humidity; and 12-h light/dark cycle with lights on at 8:00 a.m. daily). The animals were free access to standard laboratory chow and water. All experiments were carried out in accordance with the U.S. National Institutes of Health Guide for the Care and Use of Laboratory Animals (NIH Publication 85-23, revised 2011) and have been approved by the Experimental Animal Care and Use Committee of Nanjing University. All efforts were made to minimize the number of animals used and their suffering.

METHOD DETAILS

Lentiviral transduction and stereotactic microinjection

The coding sequence of *Crf* (LV-*Crf*-RNAi) or negative control (LV-control-RNAi) was ligated into the GV118 plasmid (Genechem, Shanghai, China). The sequence for *Crf* was 5′-AGATTATCGGGAAATGAAA-3′, whereas the sequence for the control siRNA was 5′-TTCTCCGAACGTGTCACGT-3′. All correct insertions were confirmed by restriction mapping and direct DNA sequencing. Titers of concentrated viral particles were between 1×10^8 and 1×10^9 TU/mL.

The concentrated lentivirus was bilaterally microinjected into the inferior olive (IO, A −12.9, L 0.7, H 8.8) of male rats (weighing 220-260 g) mounted on a stereotaxic frame (1404, David Kopf Instruments, Tujunga, CA), according to the rat brain atlas [57]. Each injection by means of Hamilton syringes driven by an infusion pump (KDS100, KD Scientific, Holliston, MA) was 1 μL at 0.2 μl/min. After 21 days, the *Crf* mRNA level in the IO was assessed by quantitative real-time RT-PCR, and the CRF level in the cerebellar interpositus nucleus (IN) was detected by ELISA according to the manufacturer's instructions (Biovendor, Karasek, Czech Republic). Experimental conditions were repeated at least three times to account for technical and biological variation.

Quantitative real-time RT-PCR

The IO or IN tissue punches were obtained from coronal brain slices according to the rat brain atlas [57] and pooled (5 rats in each pool). Three independent groups of RNA pools were used as biological replicates. Total RNA was extracted by using TriZol reagent (Invitrogen, San Diego, CA) according to the manufacturer's instructions. The first-strand cDNA synthesis was performed using a 1 μg aliquot of total RNA, according to the protocol of M-MLV reverse transcriptase (Promega, Madison, WI). *Crf* (in the IO), *Crfr1* (in the IN), *Crfr2* (in the IN), and *gapdh* (in the IN) mRNA were detected by quantitative real-time RT-PCR using iQ SYBR Green SuperMix (Bio-Rad, Hercules, CA). The reaction mixture contained 10 μL of 2 × master mix, 2 μL of cDNA, 2 μL of each primer (5 μM) and 4 μL of distilled water. The reaction was carried out in a Bio-Rad CFX-96 Real-time PCR System (Bio-Rad, Hercules, CA) using the following parameters: 95°C for 3 min to active the hot-start iTaq DNA polymerase, followed by 40 cycles of 95°C for 15 s, 60°C for 25 s and 72°C for 1 s. The reaction program was completed by analyzing a melting temperature. For negative controls, cDNA was replaced with water.

Retrograde tracings

The experimental procedures for retrograde tracings followed our previous report [58]. Rats (weighing 220-260 g) were anesthetized with sodium pentobarbital (40 mg/kg) and mounted on a stereotaxic frame under aseptic conditions. According to the rat brain atlas [57], a glass micropipette (10-15 μm in diameter in the tip) filled within 1 μL retrograde tracer Fluoro-Gold (4% in saline; Fluorochrome, Denver, CO) was planted into the IN (A −11.4, L 1.8-2.2, H 3.8). The tracer was injected bilaterally using electrophoresis with a square wave pulse of 5-10 μA at a rate of 7 s on/7 s off for 30 min. The glass micropipette was hold for 5 min after the injection. The immunohistochemical experiment was performed 3 weeks later to determine the injection site and location of retrogradely labeled cells. Experimental conditions were repeated at least three times to account for technical and biological variation.

Immunofluorescence

Rats (220-260 g) were deeply anesthetized with sodium pentobarbital (65 mg/kg) and perfused transcardially with 100 mL normal saline, followed by 250-300 mL 4% paraformaldehyde in 0.1 M phosphate buffer. The brain was gently removed, trimmed, and post-fixed in the same fixative for 12 hr at 4°C and then cryoprotected with 30% sucrose for 48 hr. Frozen coronal sections (25 μm thick) containing the IO or IN were acquired by using a freezing microtome (CM 3050S, Leica, Wetzlar, Germany) and mounted on gelatin-coated slides. The slices were rinsed with PBS containing 0.1% Triton X-100 and then incubated in 10% normal bovine serum in PBS containing 0.1% Triton X-100 for 30 min. Sections were incubated overnight at 4°C with primary antibodies: goat anti-CRF (1:200; Santa Cruz Biotech, Dallas, TX), rabbit anti-calbindin (1:1000; Millipore, Billerica, MA), rabbit anti-Fluoro-Gold (1:2000; Millipore, Billerica, MA), goat anti-CRFR1 (1:200; Abcam, Cambridge, MA), rabbit anti-CRFR2 (1:200; Abcam, Cambridge, MA), mouse anti-glutamate (1:500; Millipore, Billerica, MA), and/or mouse anti-GAD67 (1:500; Millipore, Billerica, MA). After a complete wash in PBS, the sections were incubated in the related Alexa 488- and/or 594-conjugated secondary antibodies (1:2000; Invitrogen, San Diego, CA) for 2 hr at room temperature in the dark. The slices were washed and mounted in Fluoromount-G mounting medium (SouthernBiotech, Birmingham, AL). Incubations replacing the primary antiserum with control immunoglobulins and/or omitting the primary antiserum were used as negative controls. The micrographs were taken with inverted laser scanning confocal microscope FluoView FV1000 (Olympus, Tokyo, Japan) or TCS SP8 (Leica, Wetzlar, Germany). Digital images from the microscope were recorded with FV10-ASW 3.1 (Olympus, Tokyo, Japan) or LAS X Viewer Software (Leica, Wetzlar, Germany). Experimental conditions were repeated at least three times to account for technical and biological variation.

Stereotactic cannula placement and behavioral tests

Male rats weighing 220-260 g were anesthetized with sodium pentobarbital (40 mg/kg) and mounted on a stereotaxic frame for brain surgery under aseptic conditions. Two stainless-steel guide tubes (length 8 mm, o.d. 0.8 mm, i.d. 0.5 mm) were implanted into the bilateral cerebellar INs of each animal. According to the rat brain atlas [57], the lower ends of the guild tubes were positioned 2 mm above the cerebellar IN (A −11.4, L 1.8-2.2, and H 3.8). After the implantation, rats were housed individually and allowed to recover for at least 72 hr. During the behavioral tests, two stainless-steel injection cannulae (length 10 mm, o.d. 0.5 mm, i.d. 0.3 mm) were inserted to protrude 2 mm beyond the tip of the guide tubes, just above the cerebellar INs (for minimizing lesions of the nuclei) for microinjection of CRF (0.2 nmol; Millipore, Billerica, MA), antalarmin (selective CRFR1 antagonist, 0.5 nmol; Tocris, Bristol, UK), antisauvagine-30 (selective CRFR2 antagonist, 0.5 nmol; Tocris, Bristol, UK) or saline using Hamilton syringes (1 μL each side, lasting 2 min).

The animals used in behavioral tests were randomly grouped by different treatments. All behaviors were scored by experimenters who were blind to the treatment of the animals. All behavioral trainings/tests started at the same time (10:00 a.m.) each day. In order to achieve a stable motor performance on the rota-rod and balance beam, each animal was trained daily for at least 10 trials for 3 to 5 consecutive days before test as we previously reported [19–21].

Footprint test

We evaluated walking pattern and gait kinematics of the tested animals by a footprint test. In this test, rat hindpaws were painted with nontoxic inks. The rats were allowed to freely traverse a clear plexiglass tunnel (100 cm × 10 cm × 10 cm), with a sheet of white absorbent paper (100 cm × 10 cm) placed at the bottom of the track and a darkened cage at the end. The resulting tracks provide the spatial relationship of consecutive footfalls from which the stride length and width were measured as previously described [18, 59].

Rota-rod test

The test was performed to assess motor coordination and balance of rodents [21, 58]. Each rat was placed in an individual compartment of the rota-rod treadmill (Model 7750, Ugo Basile, Varese, Italy) and was required to keep walking to avoid falling off the device. Animals were first habituated at a low rotation speed (4 rpm) for 30 s, and then the rod was constantly accelerated to 60 rpm in 180 s. The time taken for the rat to fall off was recorded. For this test, three trials with a 3 min resting were carried out for each rat to reduce stress and fatigue.

Balance beam test

We also used a balance beam test to assess motor balance and coordination of rats [21, 58]. The balance beam was a rod with length of 160 cm and diameter of 2.5 cm. A plastic platform (7 cm × 4 cm) was set at one end of the rod as the start, and a black plastic box (15 cm × 15 cm × 8 cm) was set at the other end as a nest for motivating the animal to cross the beam. The apparatus was suspended 90 cm above a cushion to protect the fallen animals from injury. Three consecutive trails with a 90 s interval were carried out for each animal.

Whole-cell patch clamp recordings on brain slices

Whole-cell patch clamp recordings on brain slices were performed as previously described [19, 20, 60]. After decapitation under sodium pentobarbital (40 mg/kg) anesthesia, the slices (300 μM in thickness) containing cerebellar IN were obtained with a vibroslicer (VT 1,200 S, Leica, Wetzlar, Germany) according to the rat brain atlas [57], and incubated in artificial cerebrospinal fluid (ACSF) consisting of (in mM): 124 NaCl, 2.5 KCl, 1.25 NaH_2PO_4, 1.3 $MgSO_4$, 26 $NaHCO_3$, 2 $CaCl_2$ and 20 D-glucose, equilibrated with 95% O_2 and 5% CO_2, at 35 ± 0.5°C for at least 1 hr. Then the slices were maintained at room temperature. For whole-cell patch clamp recordings, the slices were transferred to a submerged chamber and continuously perfused with 95% O_2 and 5% CO_2 oxygenated ACSF at a rate of 2 mL/min maintained at 32 ± 0.5°C.

Whole-cell patch-clamp recordings were performed with borosilicate glass pipettes (3-5 MΩ) filled with an internal solution (composition in mM: 140 K-methylsulfate, 7 KCl, 2 $MgCl_2$, 10 HEPES, 0.1 EGTA, 4 Na_2-ATP, 0.4 GTP-Tris, adjusted to pH 7.25 with 1 M KOH). During recording sessions, the cerebellar IN neurons were visualized with an Olympus BX51WI microscope (Olympus, Tokyo, Japan). All images were captured with a CCD (charge-coupled device, 4912-5010, Cohu, Poway, CA), displayed on a television monitor and documented in a laboratory computer. Patch-clamp recordings were acquired with an Axopatch-700B amplifier (Axon Instruments, Foster City, CA) and the signals were fed into a computer through a Digidata-1440A (Axon Instruments, Foster City, CA) for data capture and analysis (pClamp 10.0, Axon Instruments, Foster City, CA). Neurons were held at a membrane potential of −60 mV and characterized by injection of rectangular voltage pulse (5 mV, 50 ms) to monitor the whole-cell membrane capacitance, membrane resistance and series resistance. Neurons were excluded from the experiments if the series resistance was not stable or exceeded 20 MΩ.

We assessed the responses of the recorded cerebellar IN neurons to bath application of CRFergic agents by both current clamp recordings and voltage clamp recordings. Before bath application, the whole-cell current or spontaneous firing rate of the recorded neuron was observed for at least 20 min to assure stability. After each brief stimulation (1 min) of CRF (100-1000 nM), cells were given at least 20 min for recovery and prevention of desensitization. Tetrodotoxin (TTX, 0.3 μM; Alomone Labs, Jerusalem, Israel), NBQX (AMPA/kainate receptor antagonist, 20 μM; Tocris, Bristol, UK), D-AP5 (NMDA receptor antagonist, 50 μM; Tocris, Bristol, UK) and gabazine ($GABA_A$ receptor antagonist, 50 μM; Tocris, Bristol, UK) were applied to examine the direct postsynaptic effect of CRF. To explore the underlying receptor and ionic mechanisms, selective CRFR1 antagonist antalarmin (300 nM), selective CRFR2 antagonist antisauvagine-30 (100 nM), selective CRFR1 agonist stressin-I (300 nM; Tocris, Bristol, UK), selective CRFR2 agonist urocortin-II (UCN-II, 300 nM; Phoenix, Burlingame, CA), selective inward-rectifier K^+ channel blocker tertiapin-Q (100 nM; Tocris, Bristol, UK), and selective HCN channel blocker ZD7288 (50 μM, Tocris, Bristol, UK) were used. The receptor antagonist or ion channel blocker was given for at least 15 min before we observed its effect.

According to the different electrophysiological properties combined with morphological characteristics [20, 27–29], all the recorded cerebellar IN neurons were identified and categorized into two classifications, projection neurons and interneurons. Recorded neurons with the diameter larger than 20 μm; the membrane capacitance (C_m) higher than 150 pF; the spontaneous action potential showing a complex waveform of afterpotentials marked by a fast afterhyperpolarization (AHP), an afterdepolarization, and then a slow AHP, were classified as projection neurons (Figure 3A). On the contrary, neurons with the diameter smaller than 10 μm, the C_m lower than 40 pF, the afterpotential only showing a slow AHP, were categorized as interneurons (Figure 3B).

Furthermore, to determine the characteristic of whole cell current induced by separate activation of CRFR1 or CRFR2, in voltage-clamp recordings, current-voltage plots (*I-V* curves) were obtained before and during application of stressin-I or UCN-II using a slow ramp command ($dV/dt = -10\ mV \cdot s^{-1}$, ranged from −60 to −120 mV) to allow for attainment of steady-state conditions. In addition, to examine the effect of stressin-I on HCN channel current, *I-V* curves were obtained before and during stressin-I application using a series of 1 s hyperpolarizing voltage steps (ranging from −60 to −120 mV in 10 mV steps). The depolarizing voltage sag generated by activation of the HCN channel in response to a hyperpolarizing current stimulation (80-150 pA, 1 s) in the absence and presence of stressin-I was measured in current-clamp recordings.

Rat model of cerebellar ataxia

According to the classical protocol [32, 33], we injected intraperitoneally 3-acetylpyridine (3-AP, 40 mg/kg; Sigma-Aldrich, St. Louis, MO), a neurotoxin that specifically destructs the IO neurons in brainstem without affecting the cerebellum, in male rats (weighing 220-260 g) to establish a rat model of cerebellar ataxia. Immunostaining for calbindin-positive neurons in the IO combined with behavioral assessment was employed to identify the model.

Histological identification

On the last day of the behavioral tests, the animals were deeply anaesthetized with an overdose of sodium pentobarbital, and then two insulated stainless steel wires (o.d. 0.4 mm) with 0.2 mm exposed tip were inserted (10 mm) into the cerebellar IN under guidance of guide tubes for depositing iron at the site of injection by passing DC current (10 μA, 20 s). The brain was then removed and fixed with 4% paraformaldehyde containing 1% potassium ferrocyanide. A week later, frozen serial coronal sections (50 μm thick) were prepared, performed with Nissl-staining and the dark blue dots indicating injection sites were identified according to the rat brain atlas [57]. Data from rats in which the injection sites were deviated from the IN were excluded from further analysis.

QUANTIFICATION AND STATISTICAL ANALYSIS

Statistical parameters including the definitions and exact value of *n* (number of animals or neurons, depending on the types of experiments), deviations, *p* values, and the types of the statistical tests are provided in the Figures and corresponding Figure Legends. All data were analyzed using SigmaPlot 12.5 (Systat Software, San Jose, CA) or SPSS 22 (SPSS, Chicago, IL) and expressed as mean ± SEM. The normality of data was assessed by Shapiro-Wilk test. Paired or unpaired 2-tailed Student's t test, one-way and repeated-measures two-way analysis of variance (ANOVA), and Newman-Keuls post hoc test were employed for statistical analysis. *P*-values of < 0.05 were considered to be significant.

Current Biology, Volume *27*

Supplemental Information

Role of Corticotropin-Releasing Factor in Cerebellar Motor Control and Ataxia

Yi Wang, Zhang-Peng Chen, Qian-Xing Zhuang, Xiao-Yang Zhang, Hong-Zhao Li, Jian-Jun Wang, and Jing-Ning Zhu

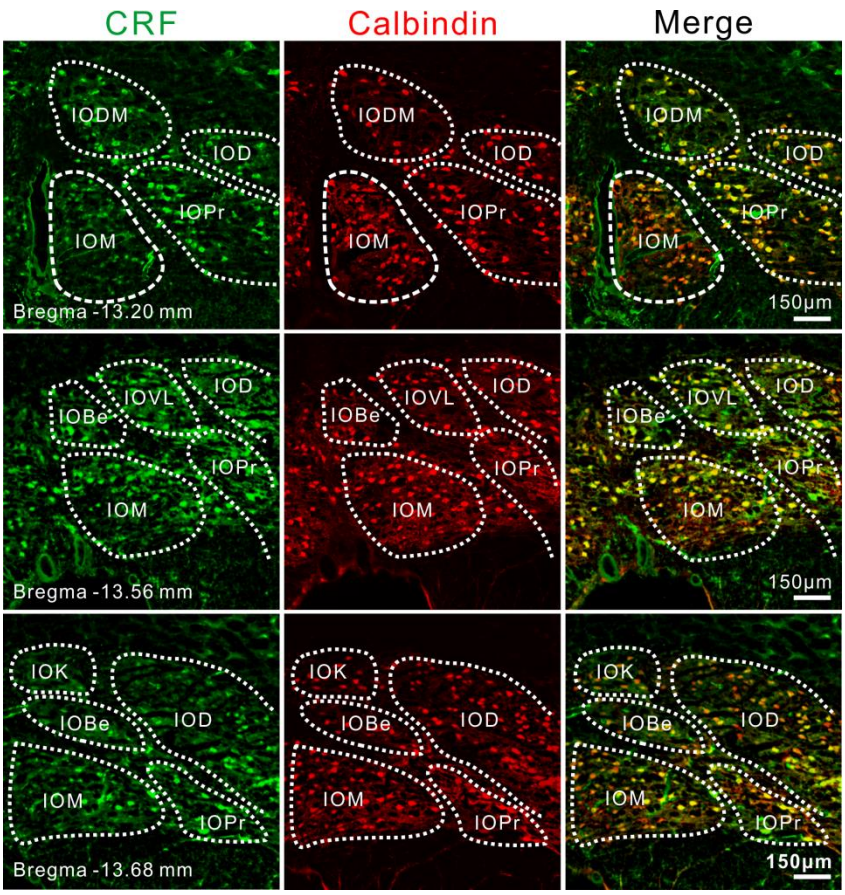

Figure S1. Distribution of CRFergic neurons in the subnuclei of the IO. Related to Figure 1.

CRF and calbindin were co-localized in neurons of all subnuclei of the IO.

IOBe, inferior olive β nucleus; IOD, inferior olive dorsal nucleus; IODM, inferior olive dorsomedial cell group; IOK, inferior olive dorsal cap of Kooy; IOM, inferior olive medial nucleus; IOPr, inferior olive principal nucleus; IOVL, inferior olive ventrolateral outgrowth.

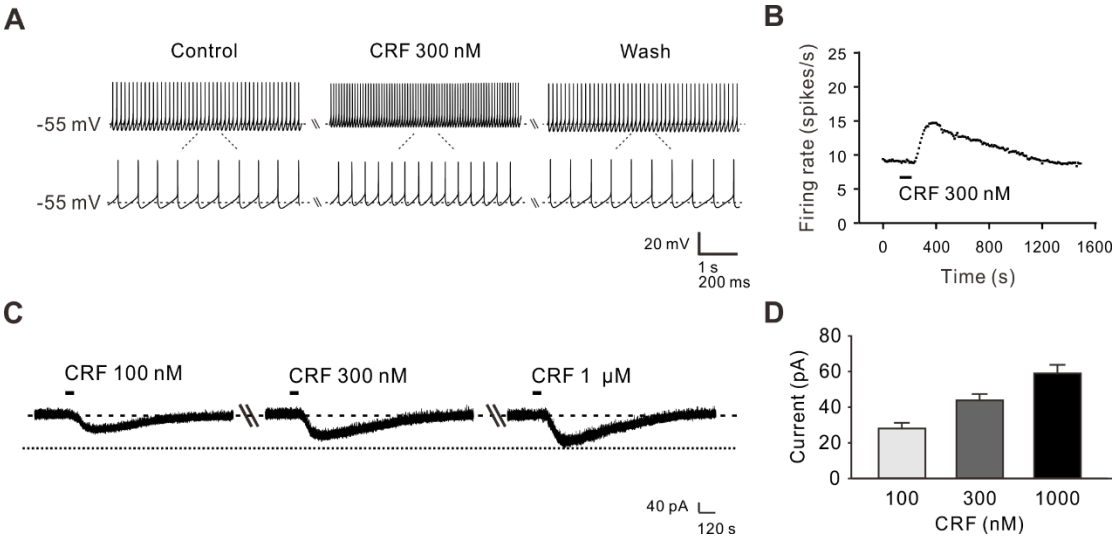

Figure S2. CRF excites projection neurons in the cerebellar IN in a concentration dependent manner. Related to Figure 3.

(A) The effect of CRF on firing rates of a projection neuron in the cerebellar IN in current clamp recordings.

(B) The PSTH showed that CRF increased the firing rates of the IN neuron presented in (A).

(C) CRF concentration-dependently elicited inward currents in an IN neuron.

(D) Group data of the tested IN neurons (n = 6).

Data represent mean ± SEM.

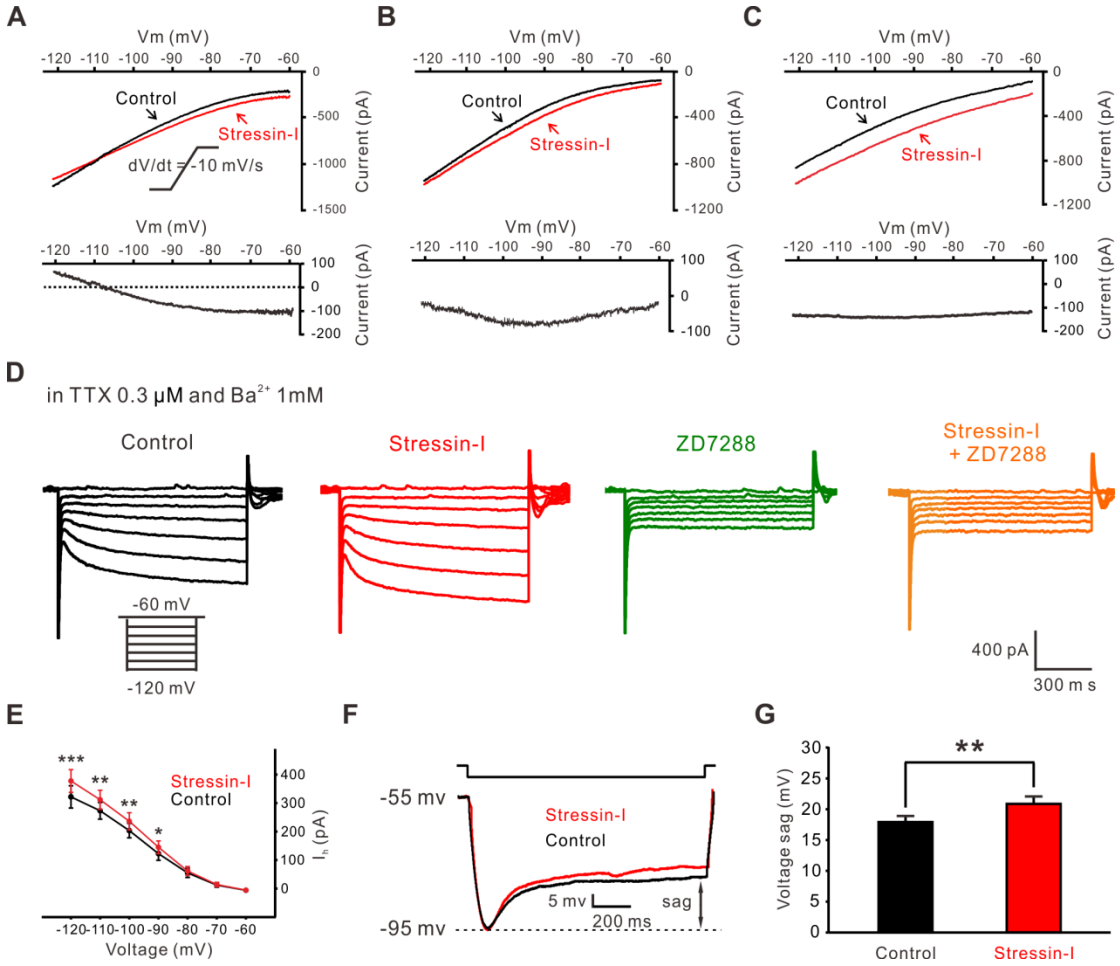

Figure S3. A dual ionic mechanism, including the closure of inward rectifier K^+ channel and activation of HCN channel, mediated the excitatory effect of CRFR1 activation on IN projection neurons. Related to Figure 3.

(A) In 33% (5/15) of the tested neurons, stressin-I (selective agonist for CRFR1) induced an inward current reversed at the calculated E_k of −105 mV. The difference current obtained by subtracting the control current from the current recorded during stressin-I application showed a strong outward rectification, indicating an involvement of inward rectifier K^+ channel.

(B) In 40% (6/15) of the tested neurons, stressin-I induced an inward current exhibiting a significant feature of hyperpolarization activated current via HCN channel.

(C) In 26.7% (4/15) of the tested neurons, the stressin-I-elicited current was similar in amplitude at −60 and −120 mV.

(D) In TTX and Ba^{2+}, a series of 1 s hyperpolarizing voltage steps (ranging from −60 to −120 mV in 10 mV steps) were employed to observe the effect of stressin-I (300 μM) on the hyperpolarization-activated currents. Stressin-I increased the hyperpolarization-activated currents which were blocked by ZD7288 in both absence and presence of stressin-I.

(E) Group data of the tested neurons (n = 6) showed that stressin-I increased the hyperpolarization-activated current, suggesting that HCN channel underlies the excitation of IN projection neurons mediated by CRFR1 activation.

(F) The IN neurons displayed an inward rectification (sag) in response to a hyperpolarizing current stimulation. Stressin-I increased the amplitude of the voltage sag.

(G) Group data of the depolarizing sag of the tested IN neurons in the absence and presence of stressin-I (n = 6).

Data represent mean ± SEM; *P < 0.05, **P < 0.01, ***P < 0.001, by paired 2-tailed student's t test (E and G).

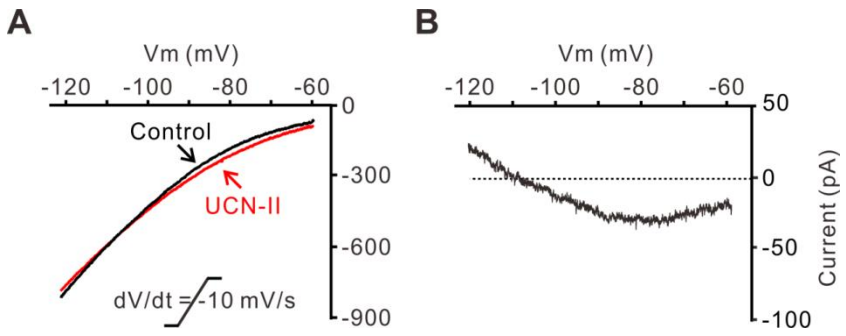

Figure S4. The change in the *I-V* curves induced by activation of CRFR2 on the cerebellar IN projection neurons. Related to Figure 3.

(A) In the tested 6 neurons, the current induced by UCN-II on the IN neurons reversed at the calculated E_k of −105 mV.

(B) The UCN-II-induced current, the difference current obtained by subtracting the control current from the current recorded during UCN-II application, showed a strong outward rectification, indicating an involvement of inward rectifier K^+ channel.